Numerical modeling of the forging process of rolls for rolling mills

J.-F. Charles
S. Castagne
L. Zhang
A.-M. Habraken
S. Cescotto
MSM Department, University of Liege, Belgium.

ABSTRACT: This article presents comparisons of forging processes between two flat tools, between two round tools, and at different forging temperatures. Simulation results help to recover and better understand long practice in the forging industry.

1 INTRODUCTION

MSM Department of Liège University and Forcast Belgium SA work together since 1996 to define a model of forging process.

The first step was to determine mechanical behavior as well as recrystallisation phenomena thanks to thermomechanical compression tests followed by microscopic investigations.

Then, the "LAGAMINE" code (Cescotto et al. 1989) was used to simulate the forging process. This non linear FEM code developed at MSM uses an elasto-visco-plastic law to compute thermomechanical analysis coupled with recrystallisation (Habraken et al. 1997).

Firstly, two-dimensional simulations have been performed but they could not represent reality. The real solicitation state is far from plane stress, plane strain or generalized plane strain where simple assumptions define the thickness of the studied slice. So, three-dimensional simulations are now performed.

A final simulation with coupling approach between thermomechanical state and recrystallisation process shows the present investigation. The final goal is a better process optimization, taking into account power limitation of the press and final microstructure of the roll.

2 NUMERICAL MODEL

2.1 *Mechanical solid law*

In solid elements, the stresses are computed by an elasto-visco-plastic constitutive law of Norton-Hoff type (Habraken et al. 1997) with thermal effects.

Its formulation is :

$$\bar{\sigma} = K_o \bar{\varepsilon}^{p4} \exp(-p_1 \bar{\varepsilon}) p_2 \sqrt{3} (\sqrt{3}\dot{\bar{\varepsilon}})^{p3} \qquad (1)$$

where $\bar{\sigma}$ and $\bar{\varepsilon}$ are respectively the equivalent Cauchy stress and strain, $\dot{\bar{\varepsilon}}$ the equivalent strain rate and K_0, p_1, p_2, p_3, p_4 are material parameters. The deviatoric visco-plastic strain rate $\hat{\dot{\varepsilon}}_{ij}^{vp}$ gives the tensorial form of this law :

$$\hat{\dot{\varepsilon}}_{ij}^{vp} = \frac{(J_2)^{\frac{1-p_3}{2p_3}} \bar{\varepsilon}^{\frac{-p_4}{p_3}} \exp(\frac{p_1}{p_3}\bar{\varepsilon})\ \hat{\sigma}_{ij}}{2(K_o p_2)^{1/p_3}} \qquad (2)$$

where $\hat{\sigma}_{ij}$ is the deviatoric stress tensor and $J_2 = \frac{1}{2}\hat{\sigma}_{ij}\hat{\sigma}_{ij}$ the second stress invariant. Such a description allows the modelization of a behavior which includes hardening and softening.

The thermal dependence of the parameters p_1 to p_4 is defined by :

$$p_4 = \text{constant} \qquad p_3 = \text{constant}$$

$$p_1 = -\left(\frac{T}{C_1}\right)^{C_2} + C_3 \qquad p_2 = \left(\frac{C_4}{T}\right)^2 + \frac{C_5}{T} + C_6 \qquad (3)$$

where T is the temperature and C_1, C_2, C_3, C_4, C_5, C_6 are material constants.

The integration is computed by an implicit method :

$$\hat{\sigma}_{ij} = 2G\left(\hat{\varepsilon}_{ij}^{total} - \hat{\varepsilon}_{ij}^{vp}\right) + \frac{1}{G}\frac{\partial G}{\partial T}\hat{\sigma}_{ij}\,\dot{T} \qquad (4)$$

or

$$\underline{\hat{\sigma}}(t) = h(\underline{\hat{\sigma}}, \bar{\varepsilon}, T) + g(t, T) \qquad (4bis)$$

where t is the time and the second order tensors are either expressed by their indicial notation or underlined.

If we suppose that we known $\underline{\hat{\sigma}}_k$ at time $t = t_o$, the difficulty is to compute $\underline{\hat{\sigma}}_{k+1}$ at time $t = t_o+\Delta t$. Developing the equation (4) in a Taylor series of first order, we found the expression giving the variation of the deviatoric stress tensor:

$$\left[\underline{\underline{I}} - \left.\frac{\partial h}{\partial \underline{\hat{\sigma}}}\right|_{t_o} .\theta.\Delta t\right]\Delta\underline{\hat{\sigma}} = \Delta t.\left[h\left[\underline{\hat{\sigma}}_k, \bar{\varepsilon}_k, T(t_o)\right] + \underline{g}(t_o + \theta\Delta t, T(t_o))\right]$$

$$+ \theta.\Delta t\left[\left.\frac{\partial h}{\partial \bar{\varepsilon}}\right|_{t_o} \Delta\bar{\varepsilon} + \left.\frac{\partial h}{\partial T}\right|_{t_o} \Delta T + \left.\frac{\partial g}{\partial T}\right|_{t_o} \Delta T\right] \qquad (5)$$

with $0<\theta<1$. Generally $\theta = 2/3$ is used.

2.2 *Computation of the dynamic recrystallised fraction (partial uncoupled approach)*

The implemented model is based on the work of Sellars and Kopp (Sellars 1969, Kopp et al. 1992-1993).

The curves $\varepsilon_C(Z)$ and $\varepsilon_S(Z)$ respectively express the limit strains for the recrystallisation beginning and end versus Zener parameter.This parameter is a function of the strain rate $\dot{\bar{\varepsilon}}$, the activation energy Q, the temperature T and the Boltzman constant R :

$$Z = \dot{\bar{\varepsilon}}\exp\left(-\frac{Q}{RT}\right) \qquad (6)$$

Experimentally defined, each curve, $\varepsilon_C(Z)$ or $\varepsilon_S(Z)$, is expressed by an analytical function depending on 4 materials parameters R_1 to R_4.

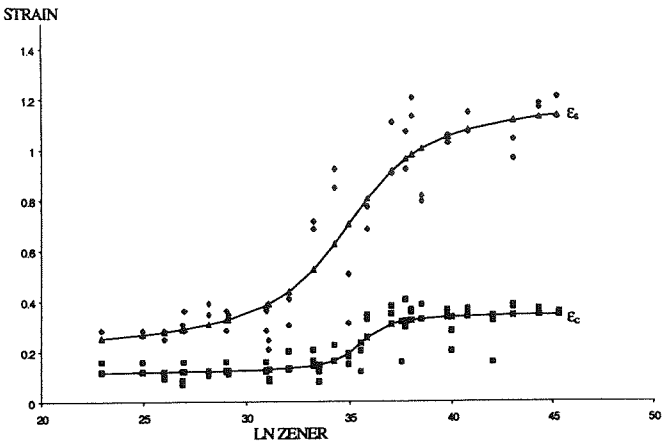

Figure 1. Example of curves defining the beginning and the end of the recrystallisation

$$\varepsilon_{C/S} = R_1 * \mathrm{ATAN}\left[\left(\ln(Z) - R_2\right) * R_3\right] + R_4 \qquad (7)$$

If Zener parameter is constant, the recrystallised fraction X_{dyn} is obtained by an Avrami law. This law is largely used to represent kinetics of metallurgical transformations such as phase transformations (austenitic, perlitic...) or static, dynamic recrystallisation. Its general form is:

$$X = 1 - \exp\left(-b\,t^n\right) \qquad (8)$$

where X is the recrystallised fraction, t is here the time from the recrystallisation beginning and b, n are material constants.

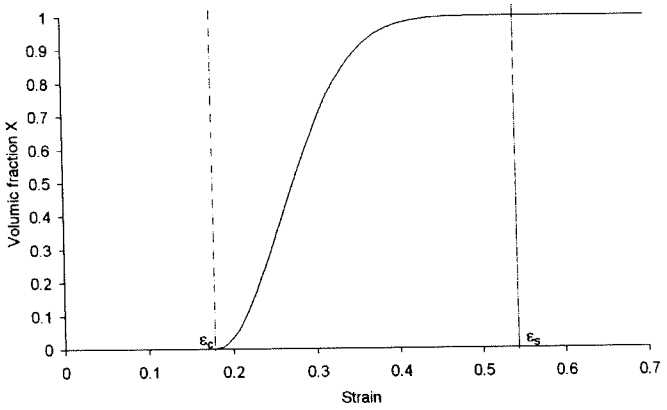

Figure 2. The Avrami law.

The structure is assumed to be completely recrystallised if the volume fraction value of 95% is reached. So the Avrami law can be written as :

$$X = 1 - \mathrm{EXP}\left[-3 * \left(\frac{\varepsilon - \varepsilon_c}{\varepsilon_s - \varepsilon_c}\right)^n\right] \qquad (9)$$

Based on Avrami approach, our computational algorithm is described hereafter. It takes into account the variation of Zener parameter during the real recrystallisation process.

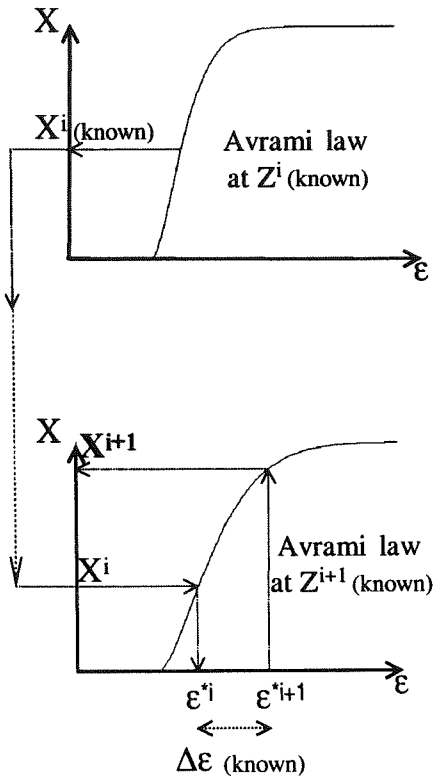

Figure 3. Recrystallised volumic fraction in case of Zener parameter variation

Let us use the subscript i to define the configuration at the step beginning and subscript i+1 to define the configuration at the end of the step.

The recrystallised fraction X^i is known and was computed during the previous step. This value is reported in the Avrami law at time i+1 and a fictive strain ε^{*i} is computed. Knowing the strain increment on the step i - i+1, we can compute the new recrystallised fraction X^{i+1} according to the Avrami law at time i+1 by using equation (9).

The recrystallised fraction for the step i - i+1 is equal to the difference between the recrystallised fraction computed at the end of the step and the one computed at the previous step.

$$DX_{dyn} = X^{i+1}_{dyn} - X^{i}_{dyn} \qquad (10)$$

The total recrystallised fraction is equal to the sum of the recrystallised fractions computed at each step, since the beginning of the simulation.

$$X^{i+1}_{dyn} = \left(1 - X^{i}_{dyn}\right) * DX_{dyn} + X^{i}_{dyn} \qquad (11)$$

This method is additive; the microstructure is directly coupled to thermal and mechanical histories of the material. However in this partially uncoupled approach, the recrystallisation process does not affect the thermal and mechanical properties.

2.3 *Total coupling case*

The principle is that each integration point of the mesh is divided into substructures (figure 4) defined by their volumic fraction A and their hardening degree directly related to the recrystallisation process and the macroscopic strain. Each substructure follows one microscopic stress curve $\underline{\sigma}_{micro}$ ($\underline{\varepsilon}_{micro}$). At the substructure birth, $\underline{\varepsilon}_{micro}$ is assumed to be zero, then it increases with macroscopic strain rate $\underline{\dot{\varepsilon}}$. So $\underline{\varepsilon}_{micro}$ plays more the role of a hardening variable than a real strain.

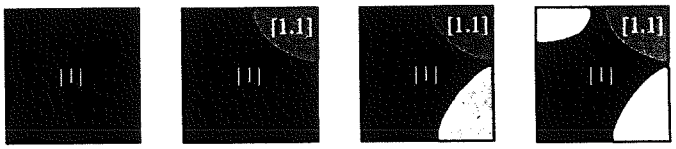

Figure 4. Integration point representation

During one time step, at each integration point of the mesh, the FEM code loops over the substructures defining this integration point and actualises, for each substructure, its stress, the strain and Zener parameter. It also checks if the recrystallisation is in progress or not, which induces death, birth or volume change of some substructures (figure 5).

So, for one substructure, four cases are possible:

- the equivalent strain is lower then ε_c : no recrystallisation, the volumic fraction of the substructure is unchanged;
- the recrystallisation occurs but it is the beginning: the phenomena is neglected because the recrystallised fraction A is smaller then the minimum fraction A_{min};
- the recrystallisation occurs and is quasi completed: the old substructure disappears and a new substructure is created;
- the recrystallisation occurs and is partial: the old substructure is kept and its volume is actualised and a new substructure is created.

At the end of the substructures loop, the macroscopic stresses are computed according to the stress in each substructure by a mixing law (figure 6).

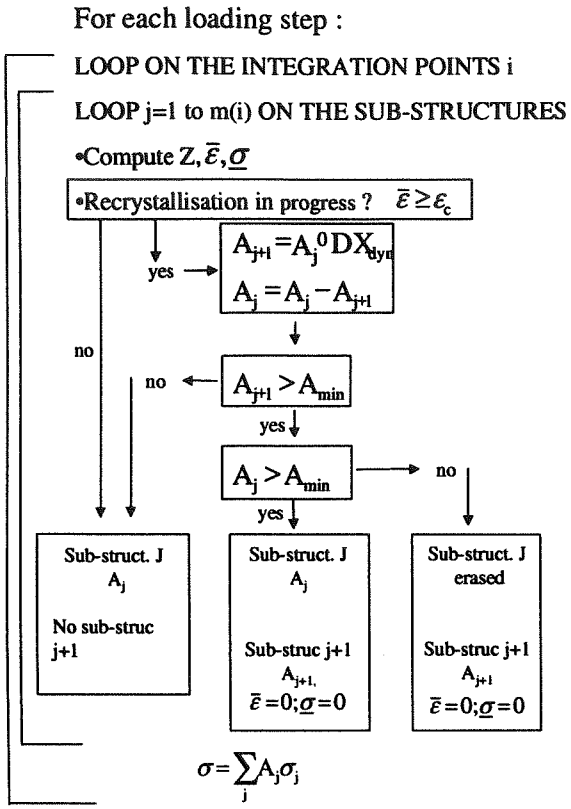

Figure 5. Actualization of the sub-structures

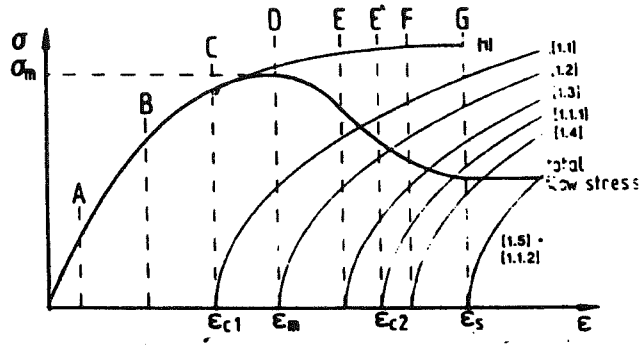

Figure 6. Sub-structure and total equivalent $\bar{\sigma}$ - $\bar{\varepsilon}$ curves.

3 HOT COMPRESSION TEST

Hot compression tests on small cylinders at different temperatures and strain rates are made till strain level from 0.1 up to 0.7. The temperature is regulated by using K type thermocouples and the heating is performed by using a quad elliptic chamber with four infrared lamps. The temperature and the strain rate $\dot{\varepsilon}$ are kept constant during the compression test thanks to regulation (see figure 7).

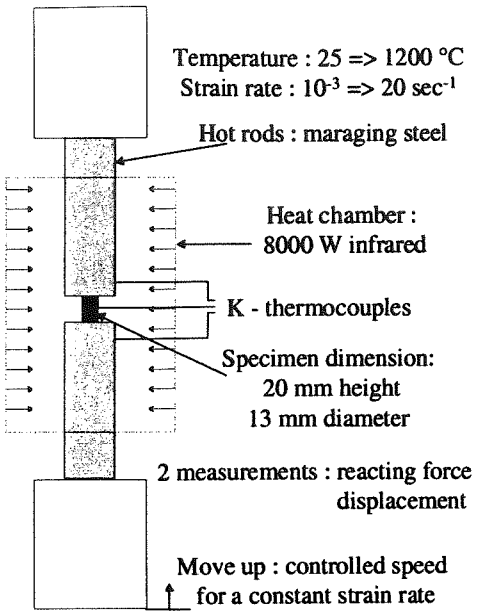

Figure 7. Hot compression test description.

Thanks to these hot compression tests, we are able to characterize the mechanical behavior of the tested forging steel. The following figure shows the obtained true stress – true strain curves.

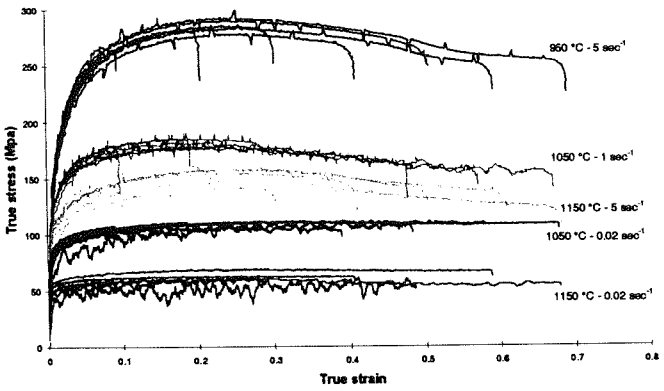

Figure 8. True stress – true strain curves of a forging steel.

A metallographic study of the quenched cylinders gives the recrystallised fraction function of the strain, the strain rate and the temperature. This study is still in progress, so the following figure does not represent the final results.

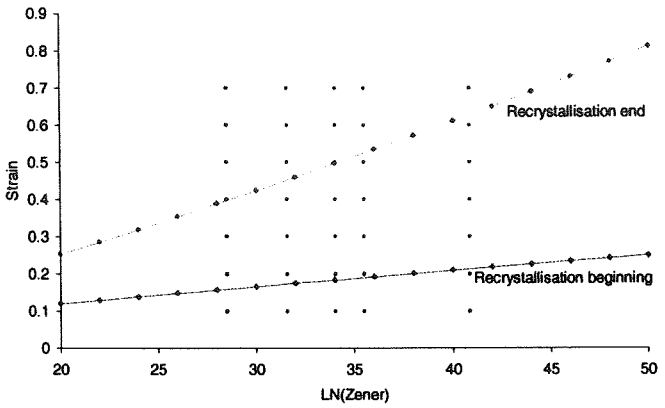

Figure 9. Recrystallisation according to the strain, the strain rate and the temperature

4 SIMULATIONS

First, a forging process of a roll was simulated in 2D. But the results obtained were not significant. So 3D simulations were necessary to be closer the reality of the phenomena as explained here under. Due to the symmetry, only a quarter of the roll is used for the mesh.

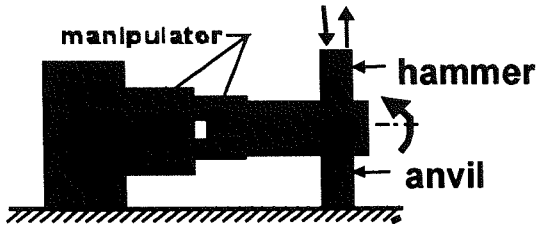

Figure 10. The studied forging process

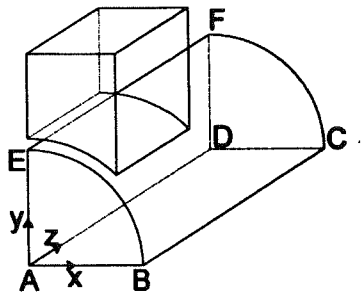

Figure 11. The symmetry.

4.1 *2D simulations*

It was impossible to simulate the forging process either in plane strain state because the solicitation is not constant along the roll or in plane stress state because of the roll length. So we tried to use a generalized plane state to simulate the process.

A slice of roll, the thickness of which is constant in space but variable in time is simulated. All the forces that are perpendicular to this slice are balanced at the level of one degree of freedom connected to the roll thickness which is constant for all the elements. These forces come from the mechanical stress field in the solid. In practice, the industrial reality shows that the thickness of the roll varies in space. In fact, the center of the roll is more deformed than its skin which is cooler and participates at the hardness of the tools. So, it was necessary to perform 3D simulations.

4.2 *3D simulations partial uncoupled approach*

In 3D simulations, we have compared the influence of the tools shape and of the initial temperature of the forged roll. If there is a cooling of the skin before forging, it participates with the tool during the forging process and the centre of the roll is more deformed, which is better. But if the cooling time is too long, the cooling benefice disappears as we see in the following results.

4 cases were simulated: the applied force is the same in each case and its maximum is equal to $4\ 10^7$ N.

- Flat tools – no cooling : the temperature is 1423 K (1150 °C) and constant in time and space;
- Round tools - no cooling : the temperature is 1423 K (1150 °C) and constant in time and space;
- Round tools - a cooling of 20 min : the initial temperature is 1423 K (1150 °C), then a thermal simulation models a 20 min cooling. The final temperature varies form 1134 (861 °C) to 1423 K (1150 °C) and is kept constant during the simulation of forging;
- Round tools - a cooling of 80 min : the initial temperature is 1423 K (1150 °C), then a thermal simulation models a 80 min cooling. The final temperature varies form 1002 (729 °C) to 1419 K (1146 °C) and is kept constant during the simulation of forging.

The displacements along the x (figures 12 to 15) and the z (figures 16 to 19) axis show that it is better to use round tools then flat ones because the displacements are more concentrated in the center of the roll and their maximum values are bigger.

Comparing the results obtained for round tools and for several cooling times, it can be seen on figures 12 to 15 and 16 to 19 that a too long cooling time is not recommended as the roll can not be forged anymore because of its too low temperature. A 20 min. cooling time seems to be better to obtain the maximum displacements along the x axis. However, looking to the z axis displacements, the gain it less.

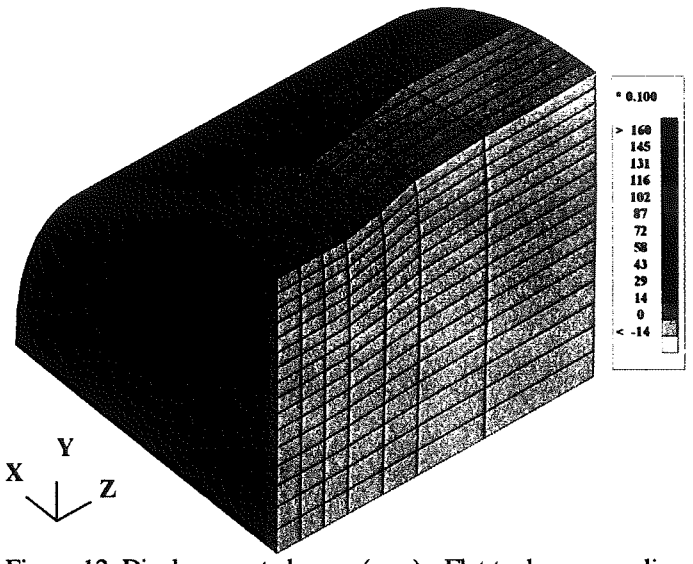

Figure 12. Displacement along x (mm) - Flat tools – no cooling – max.=14.10

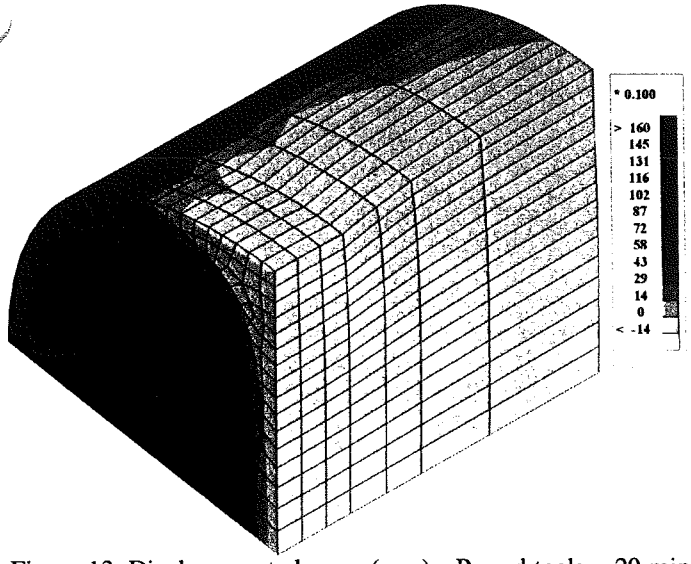

Figure 13. Displacement along x (mm) - Round tools – 20 min cooling – max.=19.10

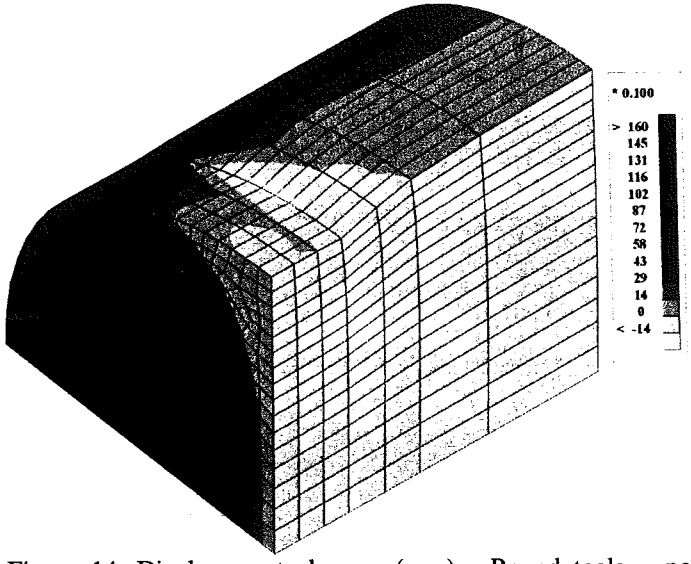

Figure 14. Displacement along x (mm) - Round tools – no cooling – max.=16.90

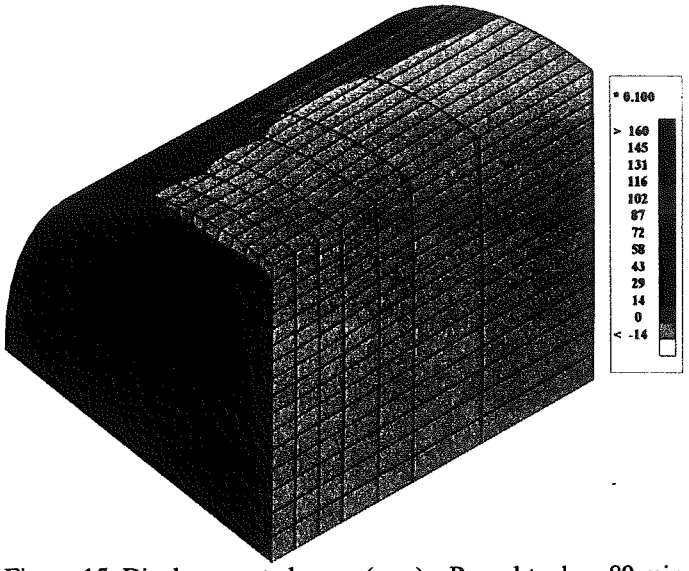

Figure 15. Displacement along x (mm) - Round tools – 80 min cooling – max.=12.40

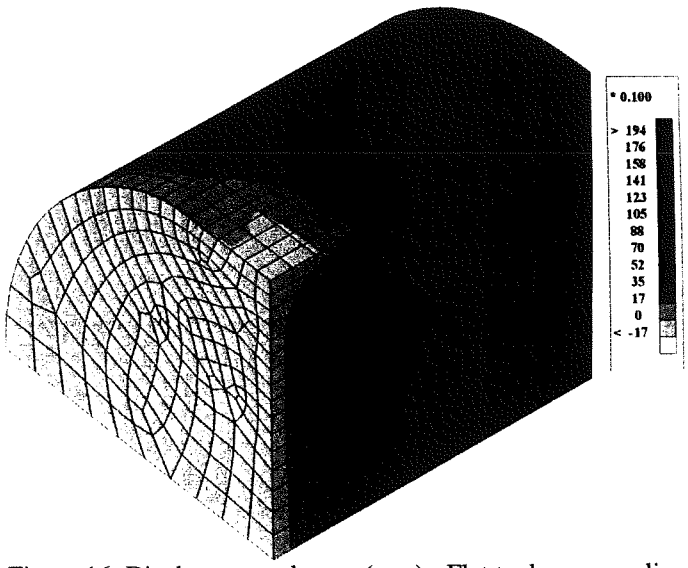

Figure 16. Displacement along z (mm) - Flat tools – no cooling – max.=16.4

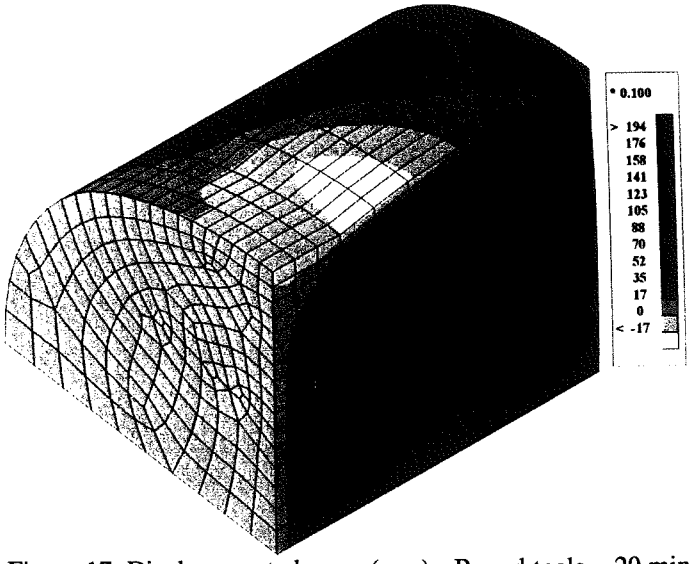

Figure 17. Displacement along z (mm) - Round tools – 20 min cooling – max.=20.2

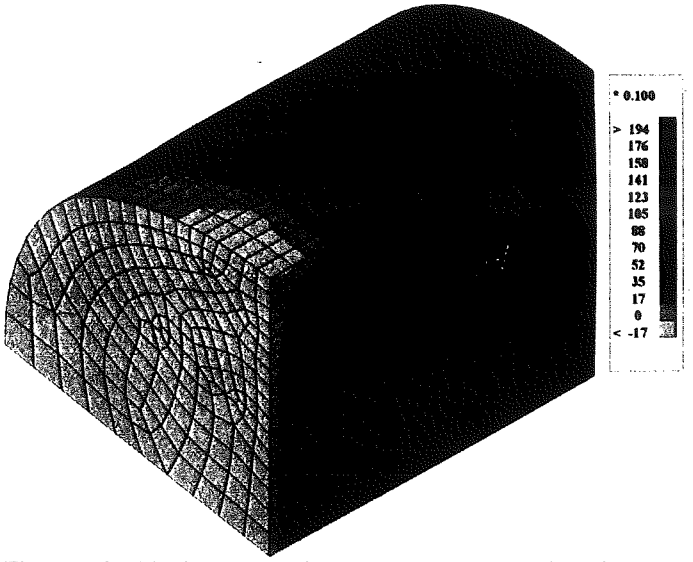

Figure 18. Displacement along z (mm) - Round tools – no cooling – max.=23.8

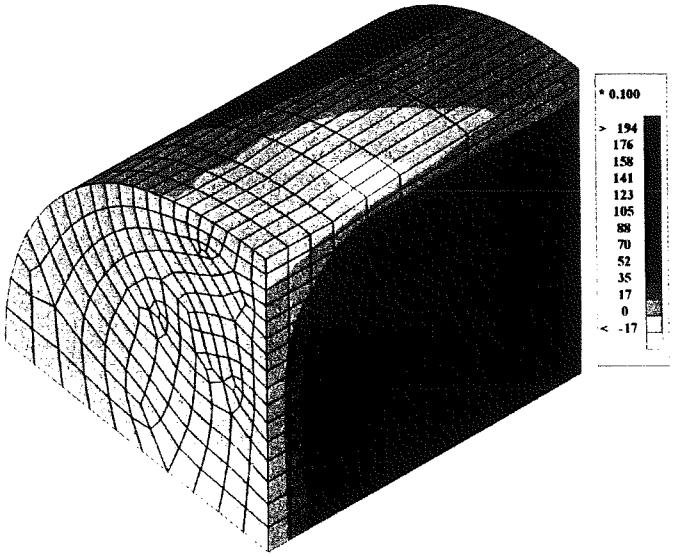

Figure 19. Displacement along z (mm) - Round tools – 80 min cooling – max.=11.3

4.3 *3D simulations with total coupled approach*

For this simulation, the same data as the case 2 (round tools – no cooling) is used but the coupling between the thermomechanical analysis and the recrystallisation is taken into account. As the recrystallisation parameters identification is still in progress, the present results are just qualitative. The displacement distributions along the x and the z axis are quite comparable with those obtained by the simulation with partial coupling. Looking at figures 20 and 21 representing the recrystallised volumic fraction, we see that there are two maximum recrystallisation zones. The first one is located under the skin of the roll where is located the end of the round tools. The second one is located in the center of the roll where the temperature is maximum.

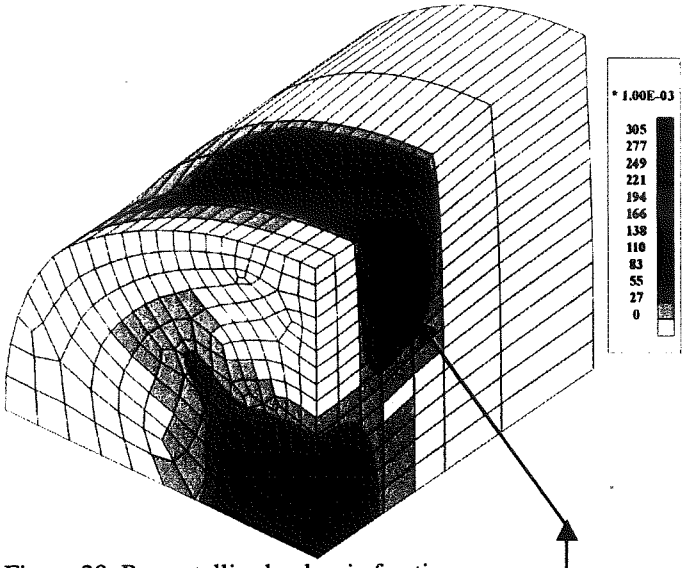

Figure 20. Recrystallised volumic fraction

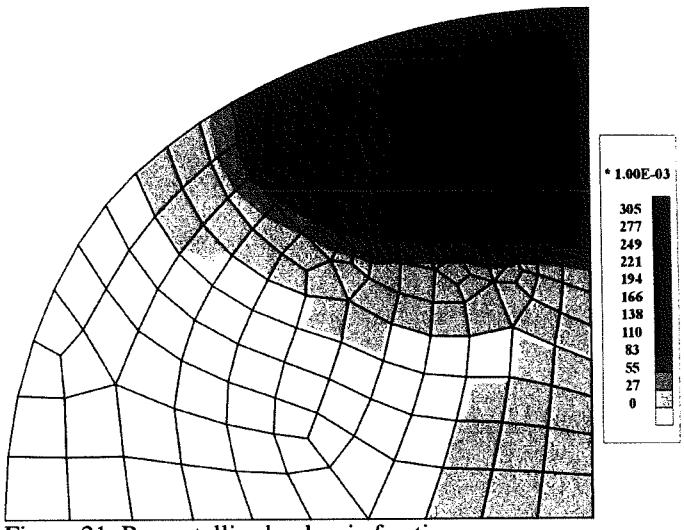

Figure 21. Recrystallised volumic fraction

5 CONCLUSION

The described elasto-visco-plastic model is able to simulate forging process of rolls. The simulations show the importance of the tools shape on the results as well as the importance of the cooling time elapsed before the forging process. For a short cooling time, the skin of the roll collaborates with the tools in the forging process which is benefit but, if the cooling time is too long, this benefit disappears due to the too low initial temperatures.

The computation of the dynamic recrystallised volumic fraction is also possible but need an important set of experiments and metallographic study to accurately identify the parameters of the model.

ACKNOLEDGMENT

The authors are pleased to acknowledge the support of their work provided by the Région Wallone, FNRS and Forcast Belgium SA

REFERENCES

S. Cescotto, A.-M. Habraken, J.-P. Radu, R. Charlier, "Some recent developments in computer simulation of metal forming process", Proc. of the 9th. Intnl. Conf. On Computer Methods in Mechanics, Vol. 4, 16-20 May 1989, Krakow, Poland.

A.-M. Habraken, J.-F. Charles, J. Wegria, S. Cescotto, "Dynamic recrystallisation during Zinc Rolling", First issue of Int. J. of Forming Processes, 1997

Sellars, Acta. Met. 17, pp1033/43 ,1969

Kopp, R & Karhausen, K, "Application of FEM and elementary theory of plasticity to prediction of microstructure in hot rolling", 1st Intnl. Conference on Modeling of Metal Rolling Processes, 1993, Imperial College

Kopp, R. & Karhausen, K., "Model for Integrated Process and Microstructure Simulation in Hot Forming", Jnl. Of Constructional Steel Research, Vol. 63, n°6, pp. 247-256, 1992